Iranian Journal of Materials Science and Engineering, Vol. 20, Number 3, September 2023
RESEARCH PAPER

Parametric Investigation of Similar TiAl6V4 and AA2024 Rotary Friction Weld Joints Using Taguchi-L9 Array Method

Houssem Eddine Lakache[1]*, Riad Badji[2], Abdelghani May[1]

* *lakache.houssem@gmail.com*

[1] Laboratoire Génie des Matériaux, École Militaire Polytechnique, BP 17, 16214, Alger, Algérie.
[2] Research Centre in Industrial Technologies (CRTI), B. P 64 Cheraga Algeria.

Received: January 2023 **Revised: August 2023** **Accepted: August 2023**
DOI: 10.22068/ijmse.3121

Abstract: *The objective underlined in this work is to apply the Rotary Friction Welding (RFW) process to joint similar AA2024 and TiAl6V4 welds. The experiment is conducted by varying the input parameters (rotational speed, friction pressure, and friction time) using Taguchi's L9 orthogonal array method. MINITAB software was used to plot the response chart. The output parameter considered in this approach is the Ultimate Tensile Strength (UTS) of the weld joint, where the optimum RFW condition for maximizing the UTS was determined. Besides, the most influential process parameter has been determined using statistical analysis of variance (ANOVA). Finally, the general regression equations of the UTS for both materials are formulated and confirmed by means of the experimental tests values.*

Keywords: *RFW, Taguchi, TiAl6V4, AA2024.*

1. INTRODUCTION

Rotary Friction Welding is a solid state welding process that generates heat through the mechanical friction between a moving part and a stationary one, accompanied by the application of lateral force. Typically, an RFW cycle can be divided into two distinct phases. The first phase, known as the friction phase, involves the production of welding heat to plasticize the material and form the flash at the interface [1]. The second phase, termed the forging phase, entails stopping the rotation while increasing the pressure. This phase is crucial for consolidating and cooling the weld [2, 3]. The quality of the RFW joint is intricately linked to the selection of various parameters, including rotational speed, friction and forging time, as well as friction and forging pressure [4, 5]. It is imperative to optimize these parameters to ensure the attainment of high mechanical properties in the RFW joints. By carefully fine-tuning these variables, the overall performance and integrity of the welded joints can be significantly enhanced. At the macro scale, the shape of the flash can provide an initial impression of the weld quality. However, to truly assess and quantify the mechanical strength of the RFW joint, it is essential to conduct thorough mechanical tests.

Aluminum alloys are frequently used as high strength to weight ratio materials in aerospace, automotive, and shipbuilding sectors. Since they have a high specific strength, an excellent corrosion resistance, and a reduced density, titanium alloys are also appealing in these fields [6].

The Taguchi statistical method [7] is a powerful tool to identify significant factors from many by conducting less number of tests [8]. This technique has been used by Kulkarni et al. [9] to optimize the MIG welding process parameters for the AA6061 alloy. Besides, the Friction Stir Welding (FSW) process parameters were optimized by the Taguchi orthogonal array for the Al–Li alloy joints [10]. Tutar et al. [11] used the Taguchi orthogonal array to estimate the contribution of each process parameter and to determine the optimum parameters to the tensile shear load of the AA3003 weld joints obtained by the friction stir spot welding process. Asmare et al. [12] deal with optimizing the FSW process by studying the tensile and hardness strengths of the AA6061-T6 FSW joints. Another research work on optimization by using the Taguchi technique for the dissimilar AA2219/AA5083 FSW joints, this study conducted to a joint efficiency of 90% of that of the AA5083 base metal [8]. The TiAl6V4 alloy has been successfully joined by the Linear Friction Welding process, where the welding parameters are carefully chosen [13-15]. Other authors have studied the effect of a single RFW process parameter on the TiAl6V4 weld joints and fixing the rest of the parameters [4, 16, 17]. Demouche et al. [18] found that the UTS of

[DOI: 10.22068/ijmse.3121]

the RFW samples increases with an increase in both friction time and pressure, up to a certain threshold. Beyond this threshold, however, the UTS starts to decrease again.

Though research work have been reported in literatures, it seems that the application of Taguchi method to optimize the RFW process parameters of the TiAl6V4 alloy and the AA2024 one has not yet been reported. The aim of this work is to investigate the influence of the parameters that govern the RFW process by performing welding tests for the TiAl6V4 alloy and the AA2024 one, to finally come out with an optimized model based on these parameters. This paper is divided into two main parts. The first part focuses on the mechanical characterization of RFW joints through tensile tests, for which an appropriate experimental plan has been prepared. The second part is dedicated to optimizing the regression models extracted using the Taguchi method, with the goal of determining the optimal values. The results obtained from this optimization process will be discussed in detail.

2. EXPERIMENTAL PROCEDURES

The materials used in this research work are the TiAl6V4 alloy and the AA2024 one, their chemical composition are indicated in Table 1. Figures 1a and 1b present the optical micrographs of the TiAl6V4 and AA2024 base materials, respectively, after undergoing a polishing and chemical etching process using reagents (1ml HF + 2ml HNO_3 + 17ml H_2O) and (2ml HF + 3ml HCl + 20ml H_2O), respectively, for a duration of 15 s. Vickers microhardness tests were carried out using a load of 500 gF for TiAl6V4 and 300 gF for AA2024.

The weld interface was traversed over a distance of ± 10 mm with a 1 mm step. The tensile test samples are machined from the RFW joints according to ISO 6892-1:2016 Standard [19]. Tensile tests are carried out at a speed of $10^{-3}s^{-1}$ on an MTS machine. Fracture surfaces were examined using ZEISS (EVO MA 25) Scanning Electron Microscope.

Table 1. Chemical composition of the TiAl6V4 alloy and the AA2024 one (weight %).

Elements	Al	Cu	Mg	C	Ti	V	Mn	Fe	Si
TiAl6V4	7.2	-	0.2	1.2	87.2	4.3	-	-	-
AA2024	92.5	3.9	1.2	-	-	-	0.7	0.5	0.6

For the TiAl6V4 alloy, a typical Ti (α + β) microstructure is observed (See Fig. 1a), where aluminum is an α-stabilizer and vanadium a β-stabilizer [20]. The microstructure is composed of a matrix with equiaxed grains of light-colored α phase, along with intergranular dark−colored grains of β phase [21]. The AA2024 alloy is an age hardening alloy rich in (Cu, Mg), its microstructure is characterized by an α matrix supersaturated with Al and a hardening θ phase rich in Cu that is randomly distributed within the α matrix as shown in Fig.1b.

The RFW operations are conducted using a machine capable of generating a maximum pressure of 30 MPa and achieving a rotational speed of 2000 rpm. The cylindrical samples for welding are prepared into Ø 15 mm × 55 mm. Initially, the two parts are brought into contact during the accosting phase as shown in Fig. 2a, Then, in the friction phase (Figs. 2b-c), a specific friction pressure P_1, is applied for a precise duration t_1.

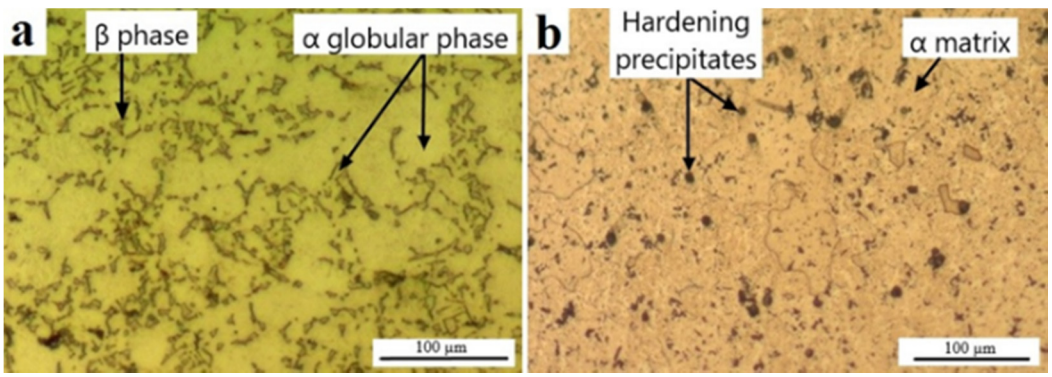

Fig. 1. Micrographs of: a) TiAl6V4 alloy and b) AA2024 alloy.

[DOI: 10.22068/ijmse.3121]

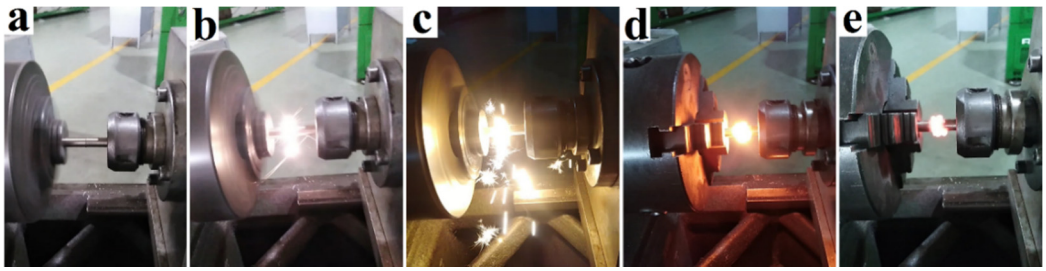

Fig. 2. Phases of RFW process during welding of TiAl6V4 sample: a) Accosting, b and c) – Friction, d and e) Forging.

The increased heat in the contact interface between the two parts leads to plastic deformation of the material, forming a flash that protrudes outward. Upon completion of the friction phase, the rotational movement is halted, marking the start of the forging phase. During this phase, the forging pressure P_2, is applied for the forging time t_2, as illustrated in Figs. 2d-e.

3. RESULTS AND DISCUSSION

In this phase, a well-structured series of tests has been meticulously conducted to identify the optimal combination of parameters that ensures the highest mechanical properties. The experimental data collected during these tests will undergo further processing at the end of this section. The subsequent analysis will involve interpreting the results and optimizing the models. For the development of the Taguchi plan, the MINITAB software has been employed as a reliable statistical tool in this study.

To achieve the optimization of RFW process parameters, three key variables, namely rotational speed, friction pressure, and friction time, have been selected for variation, as outlined in Table 2. Concurrently, the remaining parameters, specifically forging pressure (set at 5 MPa) and forging time (fixed at 6 s), are kept constant throughout the experiments. An extensive experimental plan has been meticulously designed to maximize the tensile strength of the RFW joints.

Table 2. Factors and their levels.

Factor	Level 1	Level 2	Level 3
A (rpm)	1200	1600	2000
B (MPa)	4	8	12
C (s)	4	6	8

The selection of the studied factors was conducted carefully to ensure a diverse range of tests, enabling the extraction of the individual effects of each factor. For each factor, three distinct levels were chosen based on insights gained from prior experimental tests. The experiment was meticulously designed to progress from a lower level to an intermediate level and finally to a higher level, ensuring precision and accuracy in the results obtained.

The Taguchi method provides a variety of experimental designs in the form of tables, which depend on the factors and their respective levels. For this study, the L9 model (33) was chosen, which consists of nine experimental runs with three levels for each of the three factors (as depicted in Table 3).

Table 3. L9 orthogonal arrays with tensile tests results.

Input parameters			TiAl6V4		AA2024	
A (rpm)	B (MPa)	C (s)	Sample	UTS (MPa)	Sample	UTS (MPa)
1200	4	4	T1	857.59	A1	288.59
1200	8	6	T2	912.90	A2	414.26
1200	12	8	T3	915.81	A3	429.08
1600	4	6	T4	934.88	A4	454.90
1600	8	8	T5	975.58	A5	410.56
1600	12	4	T6	972.36	A6	434.92
2000	4	8	T7	996.52	A7	401.32
2000	8	4	T8	1017.75	A8	347.17
2000	12	6	T9	1030.23	A9	460.09

[DOI: 10.22068/ijmse.3121]

Fig. 3 illustrates the RFW samples produced using the parameters mentioned in Table 3. It is evident that there is a noticeable outward material flow in the form of a flash at the weld interface. This phenomenon is a result of the substantial mechanical work combined with intense heat during the RFW process, leading to significant thermoplastic deformation.

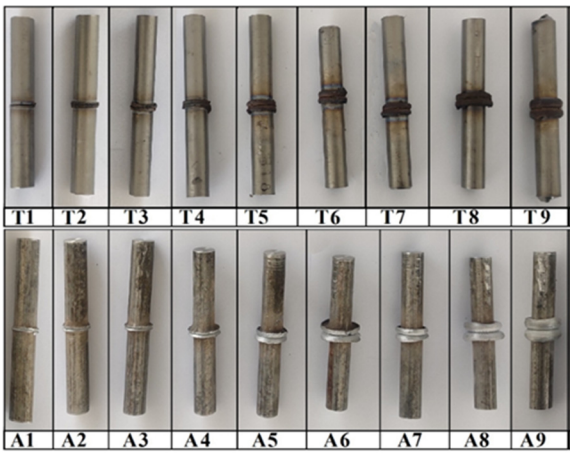

Fig. 3. RFW samples for the TiAl6V4 alloy and the AA2024 one.

The most commonly used method for the mechanical characterization of an RFW joint is to evaluate its UTS. The results of the tensile tests are presented in Fig. 4 and Table 3.

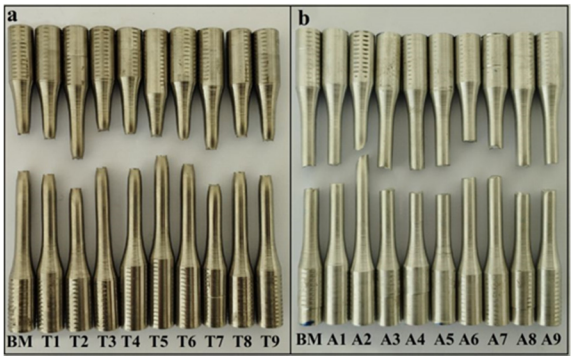

Fig. 4. Fractured tensile specimens of: a) TiAl6V4, b) AA2024.

As a reference, tests were also performed on the base metal of each alloy, yielding a UTS value of 1037.70 MPa for the TiAl6V4 alloy and 485.09 MPa for the AA2024 alloy, respectively. The fractured TiAl6V4 samples display a notable necking of the section, whereas the AA2024 alloy does not show necking. Instead, the fracture typically occurs in the center, which is the weakest area and represents the zone of stress concentration. These observations align with the findings reported by Li et al. [22].

3.1. Optimization of the RFW parameters

The recorded values of the UTS were used for the evaluation of RFW process parameters by the Taguchi method. In addition, the analysis of the factors response, as well as the variance analysis, were carried out using the MINITAB software. A confidence level of 95% is used for this study. The ANOVA analysis for the RFW process parameters is presented in Table 4, where the percentage contribution of each parameter is shown.

Among the factors investigated, the rotational speed emerges as the most influential factor affecting the UTS of the TiAl6V4 alloy, accounting for 85.10% of the variability. In contrast, the friction pressure exhibits a relatively smaller impact on the UTS, contributing to 13.51% of the total variation. The friction time, on the other hand, demonstrates a negligible effect on the UTS, with a mere 1.16% contribution to the overall variability. While the contributions in percentage of factors A, B, and C on the UTS of the AA2024 alloy are 19.74 %, 25.91 % and 47.94 % respectively. These findings indicate that each parameter exerts a distinct influence on the UTS, with friction time having the most significant impact, followed by friction pressure, and finally, rotational speed, which exhibits the lowest effect on the UTS.

The Taguchi method uses a loss function to calculate the difference between the experimental values and the desired values. This loss function is then converted into a signal-to-noise (S/N) ratio. For each level of the process parameters, the S/N ratio is calculated based on the S/N analysis. There are three types of quality characteristics in S/N ratio analysis, smaller the better, larger the better, and nominal the better. The objective of this study was to maximize the UTS. Therefore, the larger the better S/N ratio was used and calculated by the equation (1).

$$S/N = -10 * \log_{10}\left((1/N) * \sum_{i=1}^{N}\left(1/y_i^2\right)\right) \quad (1)$$

Where yi is the data observed at the ith performance characteristic, and N is the number of tests. The analysis of the effect of each control factor was performed and shown in Table 5 which shows the S/N ratios and the means response for the UTS of both materials.

[DOI: 10.22068/ijmse.3121]

Table 4. Analysis of variance for UTS.

	Source	DOF	Seq SS	Seq ADJ	Seq MS	F	P	Contribution (%)
TiAl6V4	A	2	21452.0	21452.0	10726.0	356.75	0.003	85.0956
	B	2	3404.5	3404.5	1702.2	56.62	0.017	13.5050
	C	2	292.6	292.6	146.3	4.87	0.170	1.1607
	Error	2	60.1	60.1	30.1			0.2387
	Total	8	25209.2					100
AA2024	A	2	4742	4742	2371.0	3.08	0.245	19.7386
	B	2	6224	6224	3111.9	4.04	0.199	25.9074
	C	2	11517	11517	5758.3	7.47	0.118	47.9396
	Error	2	1542	1542	770.8			6.4144
	Total	8	24024					100

Table 5. Responses of the S/N ratios and the means for the factors.

	Level	TiAl6V4			AA2024		
		A (rpm)	B (MPa)	C (s)	A (rpm)	B (MPa)	C (s)
S/N ratio	1	59.04	59.35	59.52	51.40	51.48	50.93
	2	59.65	59.72	59.63	52.73	51.81	52.92
	3	60.13	59.75	59.66	52.05	52.89	52.33
	Delta	1.09	0.40	0.14	1.33	1.41	1.99
Mean	1	895.4	929.7	949.2	377.3	381.6	356.9
	2	960.9	968.7	959.3	433.5	390.7	443.1
	3	1014.8	972.8	962.6	402.9	441.4	413.7
	Delta	119.4	43.1	13.4	56.2	59.8	86.2
	Rank	1	2	3	3	2	1

The table obtained through the Taguchi technique displays the optimal levels of the control factors. To visualize these optimal values, graphs are provided in Fig. 5a and 5b for the TiAl6V4 alloy and the AA2024 alloy, respectively. These graphs facilitate the identification of the best RFW process parameters as they highlight the highest S/N ratio for each control factor level.

Therefore the levels and S/N ratios for the factors giving the highest UTS value for the TiAl6V4 alloy were specified as factor A (Level 3, S/N=60.13), factor B (Level 3, S /N = 59.75) and factor C (Level 3, S/N = 59.66). In other words, an optimal UTS value was obtained with a rotational speed of 2000 rpm, a friction pressure of 12 MPa, and a friction time of 8 s. However, for the case of the AA2024 alloy, the factors giving the large UTS value were specified as factor A (Level 2, S/N=52.73), factor B (Level 3, S/N = 52.89), and factor C (Level 2, S/N = 52.92). This corresponds to a rotational speed of 1600 rpm, a friction pressure of 12 MPa, and a friction time of 6 s.

Regression analysis is used for modeling and analyzing relationships between multiple variables, particularly when there is a dependence on one main variable (dependent variable) and multiple other variables (independent variables). In this study, the UTS is considered the dependent variable, while the rotational speed, friction pressure, and friction time are treated as independent variables.

To obtain a predictive equation for UTS, regression analysis was used. The predictive equations for the quadratic regression of UTS for TiAl6V4 and AA2024 are given by equations (2) and (3) respectively, where A in rpm, B in MPa, C in s, and UTS in MPa.

$$\begin{aligned} UTS_{TiAl6V4}\ (Pred) &= 479.3 + 0.2654 * A \\ &+ 22.9 * B + 13.6 * C \\ &- 0.000036 * A^2 - 1.094 \\ &* B^2 - 0.85 * C^2 \end{aligned} \quad (2)$$

$$\begin{aligned} UTS_{AA2024}(Pred) &= -869 + 0.899 * A \\ &- 13.4 * B + 187.6 * C \\ &- 0.000271 * A^2 + 1.3 \\ &* B^2 - 14.45 * C^2 \end{aligned} \quad (3)$$

Fig. 6 depicts the comparison between the predicted and experimental UTS values for both materials.

[DOI: 10.22068/ijmse.3121]

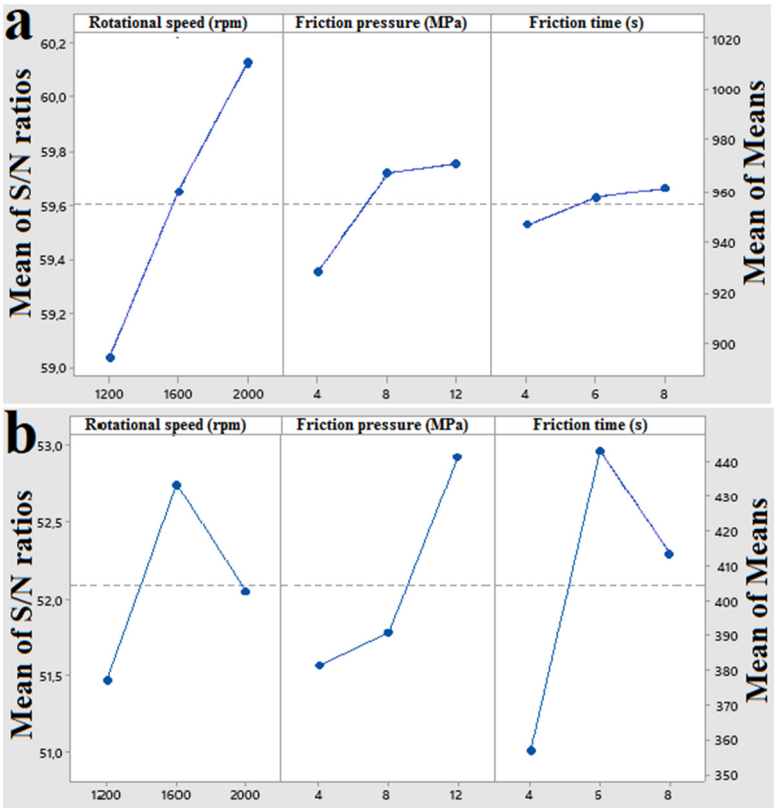

Fig. 5. Main effect plots of S/N ratios and means for the UTS of: a) TiAl6V4, b) AA2024.

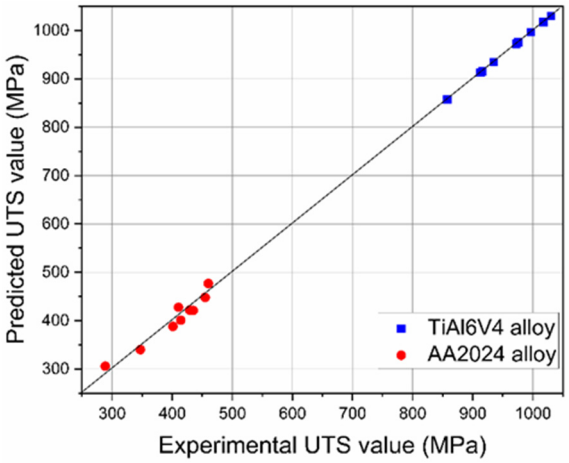

Fig. 6. Comparison of predicted end experimental UTS values for the TiAl6V4 alloy and the AA2024 one.

The validation curve for the TiAl6V4 alloy is represented by equation (4), and for the AA2024 alloy by equation (5).

The similarity coefficients, R^2(TiAl6V4) = 0.9976 and R^2(AA2024) = 0.9385, indicate a high resemblance between the predicted and experimental UTS values for the TiAl6V4 alloy. On the other hand, the AA2024 alloy exhibits relatively less resemblance between the predicted and experimental UTS values.

$$\mathrm{UTS}_{\mathrm{TiAl6V4}}(\mathrm{Pred}) = -2 + 1.0032 * \mathrm{UTS}_{\mathrm{TiAl6V4}}(\mathrm{Exp}) \quad (4)$$

$$\mathrm{UTS}_{\mathrm{AA2024}}(\mathrm{Pred}) = 25.8 + 0.9336 * \mathrm{UTS}_{\mathrm{AA2024}}(\mathrm{Exp}) \quad (5)$$

As a last step, and after extracting the UTS regression models, each model must be optimized to determine the best combination of input parameters. In order to accomplish this task, one needs to use a nonlinear programming solver as an optimization tool. In the present study, the UTS regression equations are unconstrained nonlinear functions.

The objective of our research is to maximize the UTS values for both the TiAl6V4 alloy and the AA2024 alloy by optimizing parameters A, B, and C. The solver yielded a remarkable UTS value of 1040.24 MPa for the TiAl6V4 alloy, achieved with the combination of A = 2000 rpm, B = 10.7 MPa, and C = 7.8 s. This represents a significant improvement of 100.24% compared to the UTS of the TiAl6V4 base metal (1037.70 MPa).

[DOI: 10.22068/ijmse.3121]

Thus, the optimized parameters successfully enhanced the UTS of the RFW joint.

For the AA2024 alloy, the solver yielded a UTS value of 511.92 MPa, obtained with the combination A = 1600 rpm, B = 12 MPa, and C = 6.5 s. This result represents a remarkable enhancement of 105.53% compared to the UTS of the AA2024 base metal (485.09 MPa). The optimized parameters have proven to be effective in significantly improving the UTS of the RFW joint for the AA2024 alloy as well.

3.2. Microhardness

Microhardness measurements were conducted in the vicinity of the specimens' longitudinal axis. Four lines of measurement were taken, from which average values were computed along with their standard deviations (using a t-student test at a 95% confidence level). The obtained outcomes align well with the findings reported by Skowrońska et al. [23]. In terms of TiAl6V4 microhardness profiles (depicted in Fig. 7a), a symmetrical shape is evident, characterized by a peak at the interface. Similar observations can be made for AA2024 (as shown in Fig. 7b), wherein substantial variations exist between the profiles of individual samples across different zones. These findings correspond with prior investigations concerning the TiAl6V4 alloy [24, 25] and the AA2024 alloy [26, 27].

In the case of the TiAl6V4 alloy, the microhardness measurement in the base metal yields a value of 365 HV. However, in the joint, notably high readings are evident, with values potentially soaring to 489 HV within the Fully Dynamically Recrystallized Zone (FDRZ). Conversely, hardness levels register lower within the Thermo-Mechanically Affected Zone (TMAZ) and the Heat-Affected Zone (HAZ) regions.

Shifting attention to the AA2024 alloy, microhardness data shows a peak value of 148 HV at the friction weld interface, alongside an average value of 118 HV across the TMAZ and the HAZ, a marginal reduction from the base metal's value of 125 HV. It's worth noting that the microstructural alterations triggered by the friction welding process result in diminished hardness within the HAZ [28].

3.3. Microscopic observations

Fig. 8 illustrates the optical microstructure of the TiAl6V4 weld joint. Within the FDRZ, the α phase is distinguishable by its lighter hue, set against the darker backdrop of the β phase. Moreover, an evident grain refinement is observed in both the TMAZ and the HAZ.

In Fig. 9, a detailed view of the microstructures within each zone of the AA2024 RFW joint is presented. The dynamic plastic deformation occurring in the DRZ brings about a grain refinement. Meanwhile, in the TMAZ, the grains adjust their orientation in alignment with the material flow direction.

The HAZ experiences a thermal cycle that triggers the dissolution of precipitates.

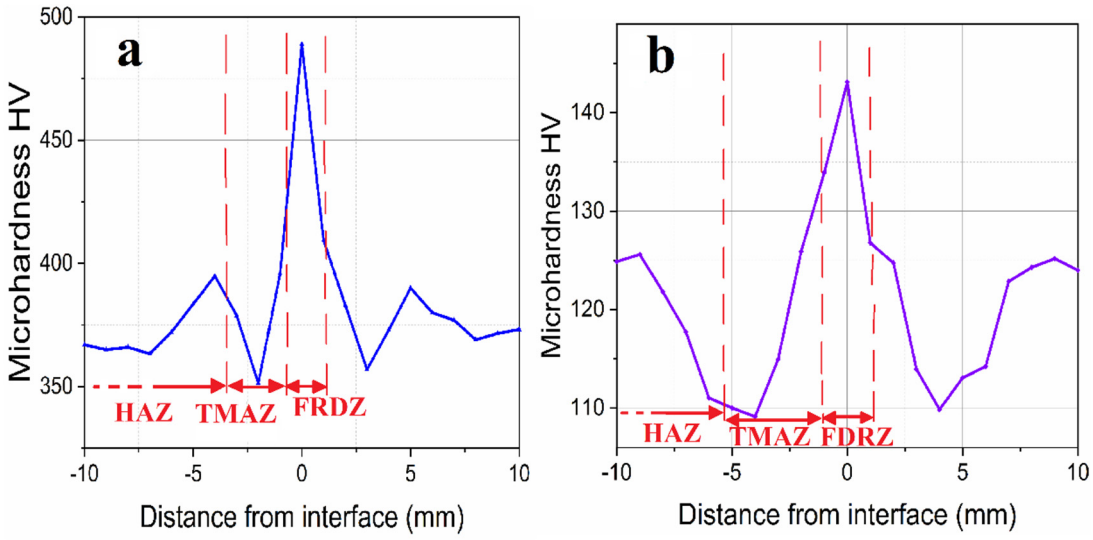

Fig. 7. Micohardness profils for: a) TiAl6V4, b) AA2024.

[DOI: 10.22068/ijmse.3121]

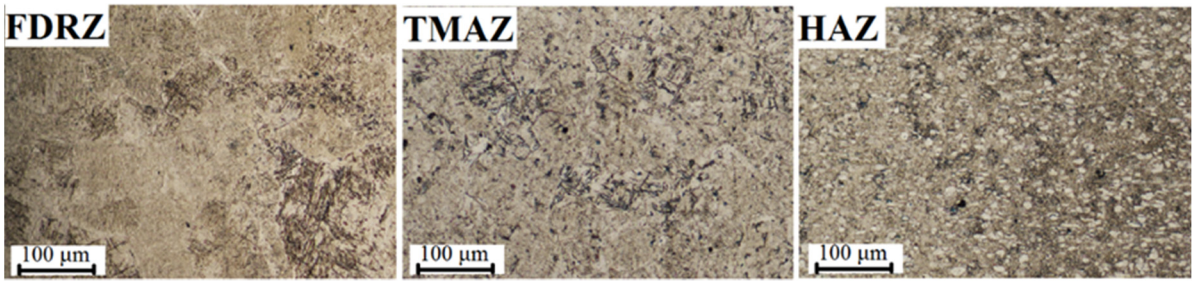

Fig. 8. Optical microstructure of the TiAl6V4 weld joint.

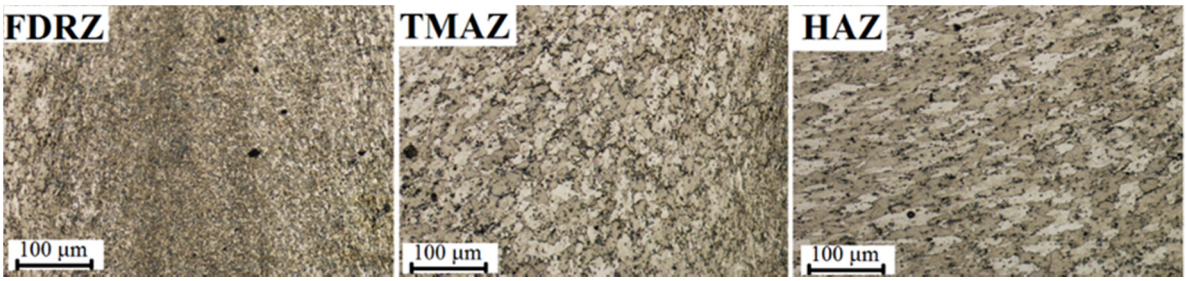

Fig. 9. Optical microstructure of the AA2024 weld joint.

Throughout the RFW process, the heat input, in conjunction with the elevated mechanical stress, prompts an inter-diffusion phenomenon of atoms at the weld interface.

It is noteworthy that diffusion bonding emerges as the primary mechanism underpinning the friction welding process, as corroborated by prior research [29]. Moreover, the process's effectiveness is significantly influenced by material mixing, serving a pivotal role in the entirety of the friction welding procedure [30, 31].

3.4. Fractographic observations

For the case of TiAl6V4 alloy, the fracture surface is reduced compared to the cross section of the tensile test specimen due to the necking phenomenon, on the contour of the fracture surface there are sharp edges like the shows Fig. 10a. To better visualize the surface, a magnification of the central zone is presented in Fig.10b. The morphology is uniform in the middle where there is a rough surface full of cupules with 10 µm average diameter as illustrated in Fig. 10c, this indicates a ductile failure mode. These results are in good agreement with the results of Vikas et al. [25]. The RFW process conditions, including rotational speed, time, and pressure, have a significant impact on the heat generated during friction. This rise in temperature transforms the material into a semi-solid state, promoting atom diffusion between the welded parts [30, 32-33], which ensure the dynamic recrystallization phenomenon of the grains.

The fracture surface of the AA2024 alloy exhibits a predominantly smooth morphology with fine dimples, as observed in Figs. 11a and 11e.

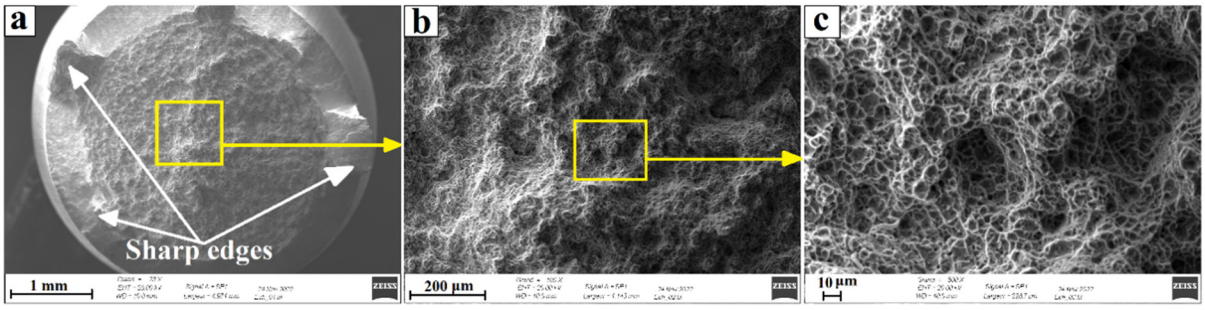

Fig. 10. a – Fracture surface of the TiAl6V4 alloy, b and c – Magnification of the central zone.

[DOI: 10.22068/ijmse.3121]

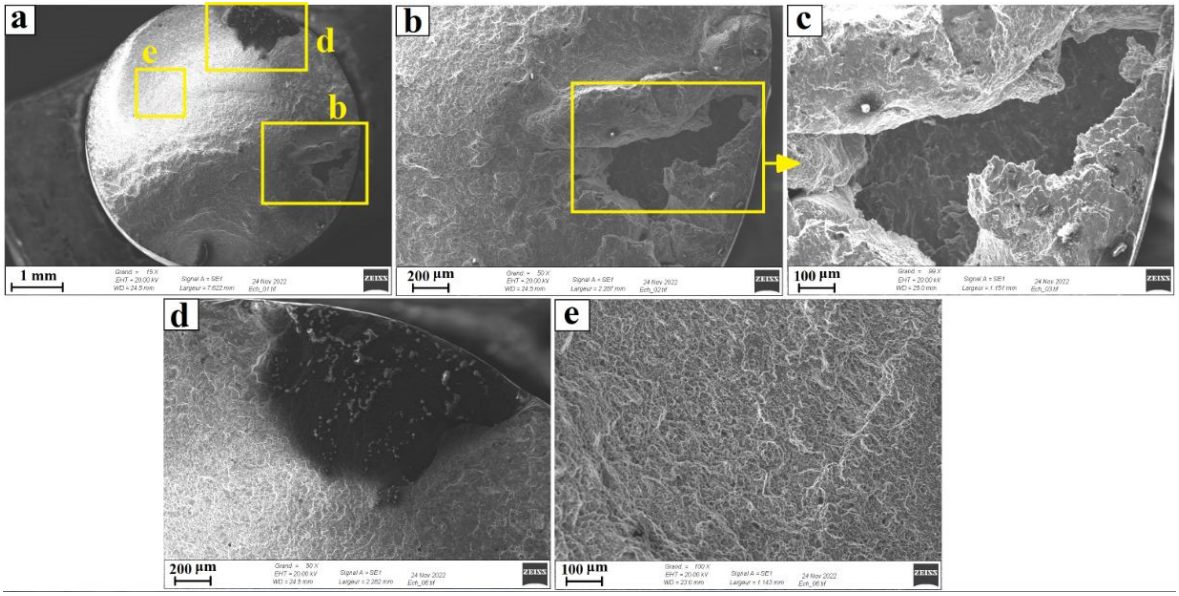

Fig. 11. a – Fracture surface of the AA2024 alloy, b, c and d – Magnification of the peripheral zone, e – Magnification of the central zone.

These fine dimples may indicate areas that were well mixed during the RFW process in the central zone. However, Fig. 11b-d present a closer view of specific regions along the periphery, showing areas that were not adequately affected by the material mixture between the two parts at the interface. Despite the lack of complete material mixing, the contact surface of the welded parts appears nearly sound. As a result, the interdiffusion phenomenon at the friction weld interface between the two parts was not fully ensured in the peripheral zone [30, 32-33].

4. CONCLUSIONS

In the present study, the RFW process was employed to join similar metals (TiAl6V4 and AA2024), using various rotational speeds, friction pressures, and friction times. The main aim was to identify the most and least influential parameters affecting the RFW joints. Based on the result analysis, the main obtained conclusions can be summarized as follow:

1. The Taguchi method was employed for the optimization of the RFW process parameters through a carefully designed experimental plan. This approach was adopted after conducting the tensile tests and gathering relevant results during the pre-treatment phase.
2. Parameter that affects mostly the UTS value of the TiAl6V4 alloy is the rotational speed.
3. The AA2024 alloy UTS is sensitive to each studied parameter of the RFW process, especially the friction time, which has the most important effect.
4. The fracture surface of the TiAl6V4 alloy showcases dimples of various sizes distributed across the entire fractured area, indicative of a ductile fracture mode. Conversely, for the AA2024 alloy, a blend of morphologies was noted, with a dominant copular surface, pointing towards a quasi-ductile fracture mode.

REFERENCES

[1]. Lakache, H. E., May, A., and Badji, R., "Rotary friction welding parameters effects upon mechanical properties and micro-structure of AA2024 weld joints." Eng. Sol. Mec., 2023, 11(3), 291-298.

[2]. Li, W., Vairis, A., Preuss, M. and Ma, T., "Linear and rotary friction welding review." Int. Mater. Rev., 2016, 61, 71-100.

[3]. Shete, N. and Deokar, S. U., "A review paper on rotary friction welding." In International Conference on Ideas, Impact and Innovation in Mechanical Engineering, 2017, 5, 1557–1560.

[4]. Avinash, M., Chaitanya, G. V. K., Giri, D. K., Upadhya, S. and Muralidhara, B. K., "Microstructure and mechanical behaviuor of rotary friction welded titanium alloys."

[DOI: 10.22068/ijmse.3121]

In Proceedings of world academy of science, engineering and technology, 2007, 26, 1307–6884.
[5]. Selvaraj, R., Shanmugam, K., Selvaraj, P. and Balasubramanian, V., "Optimization of process parameters of rotary friction welding of low alloy steel tubes using response surface methodology." Force. Mech., 2023, 10, 100175.
[6]. Hynes, N., Velu, P. S. and Nithin, A. M., "Friction push plug welding in airframe structures using Ti-6Al-4V plug." J. Braz. Soc. Mech. Sci. Eng., 2018, 40, 1-7.
[7]. Taguchi, G., Taguchi on Robust Technology Development Methods. New York, USA, 1993, 1-40.
[8]. Koilraj, M., Sundareswaran, V., Vijayan, S. and Rao, S. K., "Friction stir welding of dissimilar aluminum alloys AA2219 to AA5083 – Optimization of process parameters using Taguchi technique." Mater. Des., 2012, 42, 1-7.
[9]. Kulkarni, S. S., Konnur, V. S. and Ganjigatti, J. P., "Optimization of Mig Welding Process Parameters with Grey Relational Analysis for Al 6061 Alloy." Weld. Int., 2022, 1-14.
[10]. Alam, M. P. and Sinha, A. N., "Optimization of process parameters of friction stir welding using desirability function analysis." Weld. Int., 2022, 36, 129-143.
[11]. Tutar, M., Aydın, H., Yüce, C., Yavuz, N. and Bayram, A., "The optimisation of process parameters for friction stir spot-welded AA3003-H12 aluminium alloy using a Taguchi orthogonal array." Mater. Des., 2014, 63, 789-797.
[12]. Asmare, A., Al-Sabur, R. and Messele, E., "Experimental investigation of friction stir welding on 6061-T6 aluminum alloy using Taguchi-based GRA." Met., 2020, 10, 1480.
[13]. McAndrew, A. R., Colegrove, P. A., Bühr, C., Flipo, B. C. and Vairis, A., "A literature review of Ti-6Al-4V linear friction welding." Prog. Mater. Sci., 2018, 92, 225-257.
[14]. Li, W. Y., Ma, T. J., Zhang, Y., Xu, Q. Z., Li, J. L., Yang, S. Q. and Liao, H. L., "Microstructure Characterization and Mechanical Properties of Linear Friction Welded Ti- 6Al- 4V Alloy." Adv. Eng. Mater., 2008, 10, 89-92.
[15]. Ma, T. J., Li, W. Y. and Yang, S. Y., "Impact toughness and fracture analysis of linear friction welded Ti–6Al–4V alloy joints." Mater. Des., 2009, 30, 2128-2132.
[16]. Mukhawana, D. M., Mashinini, P. M. and Madyira, D. M., "Analysis of the Microstructure and Microhardness of Rotary Friction Welded Titanium (Ti-6AL-V4) Rods." In Eleventh South African Conference on Computational and Applied Mechanics, 2018.
[17]. Lakache, H. E., May, A., and Badji, R., "Normal pressure effects upon mechanical properties and microstructure of Ti-6Al-4V and AA2024 rotary friction welds." Eng. App. Sci. Res., 2023, 50(2), 176-184.
[18]. Demouche, M., Ouakdi, E. H. and Louahdi, R., "Effect of welding parameters in the microstructure and mechanical properties of friction-welded joints of 100Cr6 steel." Iran. J. Mater. Sci. Eng., 2019, 16(3), 24-31.
[19]. EN ISO 6892 - 1. Metallic materials - Tensile testing – Part 1: Method of test at room temperature. 2016; Brussels, European Committee for Standardization.
[20]. Rossi, S., Volgare, L., Perrin-Pellegrino, C., Chassigneux, C., Dousset, E. and Eyraud, M., "Dual Electrochemical Treatments to Improve Properties of Ti6Al4V Alloy." Mater., 2020, 13, 2479.
[21]. Kherrouba, N., Bouabdallah, M., Badji, R., Carron, D. and Amir, M., "Beta to alpha transformation kinetics and microstructure of Ti-6Al-4V alloy during continuous cooling." Mater. Chem. Phys., 2016, 181, 462-469.
[22]. Li, P., Wang, S., Xia, Y., Hao, X., Lei, Z. and Dong, H., "Inhomogeneous microstructure and mechanical properties of rotary friction welded AA2024 joints." J. Mater. Res. Technol., 2020, 9(3), 5749-5760
[23]. Skowrońska, B., Chmielewski, T. and Zasada, D., "Assessment of Selected Structural Properties of High-Speed Friction Welded Joints Made of Unalloyed Structural Steel." Mater., 2022, 16(1), 93.
[24]. Zulu, M. and Mashinini. M., "Optimisation of the rotary friction welding process of titanium alloy rods." InMATEC Web of Conferences. EDP Sciences., 2021, 347, 2.
[25]. Vikas, K. S., Rao, K. S., Reddy, G. M. and

[DOI: 10.22068/ijmse.3121]

Ramana, V. V., "Influence of heat treatments on microstructural and mechanical properties of Grade 5 titanium friction welds." Eng. Res. Express., 2022, 4(2), 025053.

[26]. Mimouni, O., Badji, R., Kouadri-David, A., Gassaa, R., Chekroun, N. and Hadji, M., "Microstructure and mechanical behavior of friction-stir-welded 2017A-T451 aluminum alloy." Trans. Indian. Inst. Met., 2019, 72, 1853-1868.

[27]. Ambroziak, A., Korzeniowski, M., Kustroń, P., Winnicki, M., Sokołowski, P. and Harapińska, E., "Friction welding of aluminium and aluminium alloys with steel." Adv. Mater. Sci. Eng., 2014, , Article ID 981653, 15 pages, http://dx.doi.org/10.1155/2014/981653

[28]. Skowrońska, B., Chmielewski, T., Kulczyk, M., Skiba, J. and Przybysz, S., "Microstructural investigation of a friction-welded 316l stainless steel with ultrafine-grained structure obtained by hydrostatic extrusion." Mater., 2021, 14(6), 1537.

[29]. Dressler, U., Biallas, G, and Mercado, U. A., "Friction stir welding of titanium alloy TiAl6V4 to aluminium alloy AA2024-T3." Mater. Sci. Eng. A., 2009, 526(1-2), 113-117.

[30]. Vairis, A., Papazafeiropoulos, G. and Tsainis, A. M., "A comparison between friction stir welding, linear friction welding and rotary friction welding." Adv. Manuf., 2016, 4, 296-304.

[31]. Wang, G. L., Li, J. L., Wang, W. L., Xiong, J. T. and Zhang, F. S., "Rotary friction welding on dissimilar metals of aluminum and brass by using pre-heating method." Int. J. Adv. Manuf. Technol., 2018, 99, 1293-1300.

[32]. Hynes, N. R. J. and Velu, P. S., "Effect of rotational speed on Ti-6Al-4V-AA 6061 friction welded joints." J. Manuf. Process., 2018, 32, 288-297.

[33]. Akinlabi, E. T. and Mahamood, R. M., Solid-state welding: friction and friction stir welding processes. New York, USA, 2020, 1–145.

[DOI: 10.22068/ijmse.3121]